

Citation for published version:

Jesus Calvo-Castro, Callum J. McHugh, Andrew J. McLean, 'Torsional angle dependence and switching of inner sphere reorganisation energies for electron and hole transfer processes involving phenyl substituted diketopyrrolopyrroles; a density functional study', *Dyes and Pigments*, Vol. 113, pp. 609-617, February 2015.

DOI:

<https://doi.org/10.1016/j.dyepig.2014.09.031>

Document Version:

This is the Accepted Manuscript version.

The version in the University of Hertfordshire Research Archive may differ from the final published version. **Users should always cite the published version.**

Copyright and Reuse:

Copyright © 2014 Elsevier Ltd. All rights reserved.

This manuscript version is distributed under the terms of the Creative Commons Attribution-NonCommercial-NoDerivatives License (<http://creativecommons.org/licenses/by-nc-nd/4.0/>), which permits non-commercial re-use, distribution, and reproduction in any medium, provided the original work is properly cited, and is not altered, transformed, or built upon in any way.

Enquiries

If you believe this document infringes copyright, please contact the Research & Scholarly Communications Team at rsc@herts.ac.uk

**Torsional angle dependence and switching of inner sphere
reorganisation energies for electron and hole transfer processes
involving phenyl substituted diketopyrrolopyrroles; a density
functional study**

Jesus Calvo-Castro, Callum J. McHugh*, Andrew J. McLean*.

Corresponding author: callum.mchugh@uws.ac.uk

University of the West of Scotland, School of Science, Paisley, PA1 2BE, UK.

Tel: +44 (141) 848 3210 Fax: +44 (141) 848 3204

Abstract

Determination of inner sphere reorganisation energies is important in the development of organic charge mediating materials and electron transfer reactions. In this study, hole and electron inner sphere reorganisation energies, λ_h and λ_e respectively, have been computed for the first time for a series of structurally related diketopyrrolopyrrole (DPP) molecular motifs. Inner sphere reorganisation energies for self-exchange electron transfer reactions are calculated as being lower than those associated hole transfer processes in model planar phenyl and thiophenyl substituted DPP systems. It is found that $\lambda_e < \lambda_h$ for all planar ring / DPP core structures examined. The effect on $\lambda_{h/e}$ of non-planarity between phenyl substituents and DPP core is explored in detail. The relative ordering of λ_h and λ_e is dependent upon the torsional angle of phenyl rings and reverses at twist angles of greater than 60° such that $\lambda_e > \lambda_h$.

Keywords: diketopyrrolopyrroles; reorganisation energies; hole transfer; electron transfer; DPP

1. Introduction

Diketopyrrolopyrroles (DPPs) are widely employed in the production of pigments[1-5] and have seen a recent surge of interest as polymeric charge mediators in organic field effect transistors (OFETs)[6-13] as well as dye based solar cell technologies.[14-21] We have recently undertaken a detailed characterisation of the photophysical, photochemical and charge transfer, CT properties of single molecule DPPs in solution, the solid phase and in thin films with a view to ultimately developing novel sensor applications and electronic devices.

We report here the results of density functional theory, DFT determinations of inner sphere reorganisation energies, λ_i for charge transfer/self-exchange reactions involving several DPP derivatives as listed in Figure 1. We are particularly interested in diphenyl substituted DPPs because of the relative ease and variety of synthetic routes available as well as the significant Stokes shifts in absorption and emission that can be induced upon substitution at R1. On the other hand, nearly all DPP based organic CT device research to date has utilised thiophenyl substituents.[10-15, 17-20, 22] It was clearly of interest to compare the two motifs.

FIGURE 1 HERE

These are the first calculations of λ_i for DPPs that we are aware of. The results are of relevance to the recent growing interest in their application as CT mediators in organic field effect transistors and solar energy cells as well as in electron transfer based turn-off/turn-on fluorescent probes.

Self-exchange charge transfer reactions may be considered[23] to be the primary mediators of charge flow in organic conducting polymers and amorphous thin films. At room temperature in such environments these reactions are usually considered to involve a series of thermally activated electron and/or hole hops between adjacent charged radical ions and neutral parent species;



Reactions 1 and 2 represent electron and hole transfer respectively between two adjacent DPP molecules. Reaction 1 can be thought of as an electron hopping from the lowest unoccupied molecular orbital, LUMO of the radical anion to the LUMO of the neutral reaction partner while Reaction 2 involves the hole hopping between the radical cation and neutral molecule hole occupied molecular orbitals, HOMOs.

Rate constants, k_{CT} for both hole and electron transfer self-exchange processes can be expressed using the semi-classical form of the Marcus equation (Equation 1):[24-26]

$$k_{\text{CT}} = \frac{2\pi}{\hbar} V^2 \sqrt{\frac{1}{4\lambda k_{\text{B}} T}} \cdot \exp\left[\frac{-\lambda}{4k_{\text{B}} T}\right] \quad \text{Equation 1}$$

where k_{CT} is the rate constant for electron transfer, k_{B} and T are the Boltzmann constants and temperature respectively, λ is the reorganisation energy and V is the electronic coupling factor, sometimes referred to as the charge transfer integral, t . It can be seen that for an iso-energetic charge transfer process, k_{CT} depends only on V and λ . In turn, λ is divided into contributions from two components; inner and outer sphere reorganisation energies, λ_{i} and λ_{o} , respectively. The latter is dependent on the dielectric and polarisable properties of the medium,[24-29] the former is the energy associated with the structural changes of the reactants on progression to product geometry (and *vice versa*).[24-26, 30] The contribution to λ from λ_{i} can be significant and dominates inner sphere charge transfer processes (those CT processes where there are no solvent molecules intervening to prevent molecular contact between reactants).[23] In general, λ_{i} increases with increasing localisation of charge whether dealing with monomeric or oligomeric materials. The labels λ_{h} and λ_{e} (or $\lambda_{\text{h/e}}$) will be used in place of λ_{i} for inner sphere hole and electron transfer respectively.

Strong electronic coupling between monomer units, for example in co-facial π - π 1-D stacks ($V > k_{\text{B}}T$) as in some crystal environments, results in a lowering of λ_{i} due to charge density being dissipated

across multiple monomers in the stack.[31, 32] The single molecule/monomer calculations we report here are therefore pertinent to situations exhibiting weak electronic coupling ($V > k_B T$) between DPPs such as in amorphous thin films and solution (as well as gas) phases. They should also represent upper limits of $\lambda_{h/e}$ values of these materials in crystalline environments.[23]

Values of $\lambda_{h/e}$ for electron and hole transfer (Reactions 1 and 2 respectively) may be broken down to the sum of two contributions;[23, 30, 33, 34] the reorganisation energy for structural change from neutral species to the radical ion, $\lambda_{h/e}^{NR}$ and the concomitant, parallel reorganisation energy for structural progression from radical ion to the neutral species, $\lambda_{h/e}^{RN}$;

$$\lambda^{NR} = E_{R_{geom}}^N - E_{N_{geom}}^N \quad \text{Equation 2}$$

$$\lambda^{RN} = E_{N_{geom}}^R - E_{R_{geom}}^R \quad \text{Equation 3}$$

$$\lambda_{h/e} = \lambda_{h/e}^{NR} + \lambda_{h/e}^{RN} \quad \text{Equation 4}$$

where $E_{N_{geom}}^N$ is the energy of the neutral species at its equilibrium geometry and $E_{R_{geom}}^N$ is the energy of the neutral species at the equilibrium geometry of the charged radical ion (Equation 2). Similarly $E_{R_{geom}}^R$ corresponds to the energy of the charged radical ion at its equilibrium geometry and $E_{N_{geom}}^R$ represents the energy of the charged radical ion at the neutral reactant's equilibrium geometry (Equation 3). Therefore $\lambda_{h/e}$ can be determined by substituting in the relevant energies at the relevant geometries of the neutral and radical cation/anion species into Equations 2-4.

Structural reorganisation can also be expressed by taking the sum of the weighted contribution to individual vibrational modes to $\lambda^{NR/RN}$:[35-40]

$$\lambda = \sum S_j h \nu_j \quad \text{Equation 5}$$

where S is the vibronic coupling (weighing) factor for a given vibrational mode, j , of frequency, ν_j . Although we do not explicitly use Equation 5 to calculate $\lambda_{h/e}$ we will show that high frequency C-C stretching, torsional and out of plane bending modes all can contribute to structural reorganisation in DPPs.

If the potential energy surfaces (PESs) of both neutral and radical ion have similar curvature along the intervening CT coordinate(s) then $\lambda^{\text{NR}} = \lambda^{\text{RN}}$. Alternatively, if the two PESs have significantly differing curvatures(s) then $\lambda^{\text{NR}} \neq \lambda^{\text{RN}}$. [23] In other words, the individual contributions to $\lambda_{\text{h/e}}$ from λ^{NR} and λ^{RN} associated with a given self-exchange charge transfer process need not to be the same depending on the relative curvature(s) of the associated PESs involved. Any difference in λ^{NR} and λ^{RN} values can be accounted for in terms of changes in frequency of a key re-organisational mode between the neutral and radical ion structures as given by Equation 5. [39]

Equation 1 indicates that it is desirable to have a low value of $\lambda_{\text{h/e}}$ in order to maximise k_{CT} for any given value of V . As such, the structural dependence of $\lambda_{\text{h/e}}$ is an important consideration to take into account when developing organic based charge transfer materials. To the best of our knowledge there are no published values of $\lambda_{\text{h/e}}$ hitherto for any DPPs despite the ever-growing number of publications involving their use in CT based materials. [9-20]

The rest of the paper is laid out as follows; first, we give a brief description of the computation methods used to determine $\lambda_{\text{h/e}}$ (according to Equations 2-4). In the results and discussion section we first describe the influence of basis set and DFT employed on the computed $\lambda_{\text{h/e}}$ values of **H₂P₂DPP**. This is then followed by an examination of the effect on $\lambda_{\text{h/e}}$ of incremental (and fixed) torsional twist of the phenyl rings with respect to the DPP core for **H₂P₂DPP**. These results are compared to those of the parent **DPP** molecule and key structural factors controlling $\lambda_{\text{h/e}}$ identified. This is followed by an examination of $\lambda_{\text{h/e}}$ of **H₂P₂/T₂DPP** and **Me₂P₂/T₂DPP** where the torsional constraints are imposed in the previous calculations are lifted. The overall results are compared with those for anthracene, **anthr**, and pentacene, **pent**, as a means of benchmarking our systems against $\lambda_{\text{h/e}}$ calculations reported by other groups. Finally we summarise our conclusions; the most important being i) that $\lambda_{\text{e}} > \lambda_{\text{h}}$ for all planar DPP based geometries examined including **T₂DPPs**, ii) λ_{e} is far more sensitive to torsional twist of phenyl substituents relative to the DPP core than λ_{h} , iii) that **H₂P₂DPP** and **Me₂P₂DPP** have comparable λ_{h} values to those of **Me₂** and **H₂T₂DPPs** and ultimately, iv) variation in %HF exchange utilised in the various Density Functionals, DFs employed has a greater influence on computed values of $\lambda_{\text{h/e}}$ than basis set size at the 6-31G(d), 6-31G(d)(p) and 6-31+G(d) levels used here.

2. Computational methods

For the most part we will be employing the M06-2X density functional,[41] DF to determine energies and geometries required for the determination of $\lambda_{h/e}$ by Equations 2-4. Little variation in $\lambda_{h/e}$ values and consistent trends were observed whether using 6-31G(d), 6-31G(d)(p) or 6-31+G(d) basis sets – so unless otherwise stated 6-31G(d) can be assumed throughout. Neutral and radical ion energies and geometries were determined using restricted and unrestricted DFT methods respectively. For all radical ion species $0.75 < S^2 < 0.78$ – indicating acceptably low spin-contamination in all cases.[42-44] All unconstrained equilibrium geometries referred to in the following discussion were confirmed by IR calculations; spectra confirming real equilibrium minima by exhibiting no imaginary modes (no negative infrared frequencies observed for any equilibrium geometry).[42-44]

Most previous determinations of $\lambda_{h/e}$ values for organic charge transfer materials[23, 30-36, 38, 39, 45] have used the B3LYP density functional[46-48] which (over and above specific training set based empirical parameters) differs from M06-2X in that i) it does not conform to the free electron gas limit; namely it suffers from self-exchange, whereas the opposite is the case for M06-2X, ii) B3LYP has 20% Hartree-Fock, % HF exchange versus 54% in M06-2X. We therefore examined the influence of % HF exchange on our computed $\lambda_{h/e}$ values of **H₂P₂DPP** using the Truhlar developed DF series; M06-L,[49] M06,[41] M06-2X[41] and M06-HF[50] DFs. These DFs have 0, 27, 54 and 100% Hartree-Fock exchange present respectively. All of the M06 DF family conform to the free electron gas limit.[41]

As discussed further we found that variation in DF employed had a greater impact on our results than variation in basis set size, at least within the relatively modest basis set range employed in this study. Any differences between $\lambda_{h/e}$ results from B3LYP versus M06-2X DFs can be shown to be explained/accounted for on the basis of the variation in % HF exchange present. Finally, all of the DFs employed here were as implemented in Spartan 10 computational software.[51]

3. Results and discussion

3.1 Influence of basis set and % Hartree-Fock exchange utilised by density functional on computed $\lambda_{h/e}$ values of **H₂P₂DPP**

Table 1 lists the various DFs used together with % HF exchange employed in the functional and the various computed components comprising $\lambda_{h/e}$ based on fully relaxed, unconstrained neutral and radical ion geometries **H₂P₂DPP**. The final values of $\lambda_{h/e}$ are given in bold. The values in brackets correspond to results obtained from energy minimised geometries constrained to $\theta_1 = -\theta_2 = 0^\circ$, where θ denotes the dihedral angle between the phenyl substituents and the DPP core. Those geometries without brackets were derived from unconstrained geometry minimisation using the various DFs listed.

TABLE 1 HERE

FIGURE 2 HERE

Table 1 illustrates four key trends;

i) λ_e is always less than λ_h suggesting that for similar V values, electron transfer is favoured over hole transfer by **H₂P₂DPP**. CT in amorphous organic devices is generally thought to be governed by Marcus theory's thermally driven hops. The results suggest that **DPP** derivatives in such devices may possess enhanced intrinsic electron transport properties over hole transport. However, reported CT properties of **DPP** based devices published to date nearly all employ thiophenyl substituents rather than phenyl groups. We will compare the two motifs in following sections.

ii) For each DF, $\lambda_{\text{h}}^{\text{NR}}$ and $\lambda_{\text{h}}^{\text{RN}}$ are similar to one another as are $\lambda_{\text{e}}^{\text{NR}}$ and $\lambda_{\text{e}}^{\text{RN}}$. This indicates that the radical ion PESs lying along the CT reorganisation coordinate(s) have similar curvature to that of neutral **H₂P₂DPP**.

iii) The computed phenyl/DPP core torsional angle systematically increases from 2.4 to 11.2° as the %HF exchange composition of the DFs increases (not tabulated), yet there is little difference between $\lambda_{\text{h/e}}$ values of unconstrained or constrained results listed. This suggests that $\lambda_{\text{h/e}}$ is independent of phenyl/DPP core torsion at low degrees of twist. In other words, reorganisation about other, higher frequency vibrational modes as well as those involved in torsional motion contribute to $\lambda_{\text{h/e}}$.

iv) It is striking that $\lambda_{\text{h/e}}$ clearly increase with increasing %HF exchange in the DFs. This is observed for both unconstrained and constrained **H₂P₂DPP** geometries as listed in Table 1. Figure 2 shows the dependence of $\lambda_{\text{h/e}}$ on %HF exchange of the DF for the constrained geometries in Table 1 to avoid any ambiguity concerning torsional contributions to $\lambda_{\text{h/e}}$. Positive linearity is observed for both sets of data across the entire range of the plot with λ_{h} showing to be more sensitive to %HF exchange than λ_{e} . It is known that computed bond length alternation, BLA in π -conjugated systems is dependent on the weighing of %HF exchange in the DF used.[41, 52] Large %HF exchange results in an exaggeration of BLA in polyene π -conjugated systems whereas low %HF underestimates BLA. This problem is well known with the B3LYP DF that has been shown to underestimate BLA in conjugated polyene systems.[53] As a result of these DF associated BLA errors, those DFs listed in Table 1 with low %HF character will underestimate and those with high %HF character will overestimate C-C bond length changes, ΔBL on radical ion formation from neutral reactants. The net result is that $\lambda_{\text{h/e}}$ will be too low with the former and too high with the latter DFs respectively. Going back to Figure 2, the dependence of computed $\lambda_{\text{h/e}}$ values of %HF exchange may therefore indicate significant contributions to $\lambda_{\text{h/e}}$ from ΔBL associated with the π conjugation pathways of **H₂P₂DPP**. If so, then the relative slopes of λ_{e} and λ_{h} further suggest greater ΔBL s are associated with hole compared to electron transfer. A plot of the magnitude of the sum of ΔBL , $\Sigma|\Delta\text{BL}|$ versus %HF exchange for constrained **H₂P₂DPP** is given in Figure 3. It can be seen that a strong linear relationship is evident.

FIGURE 3 HERE

We therefore conclude that variations in $\lambda_{h/e}$ of **H₂P₂DPP** with DF given in Table 1 and Figure 2 are associated with BLA and Δ BL estimates varying with %HF exchange in the DF employed. Larger $\lambda_{h/e}$ values scale with larger computed Δ BL and lower values of both parameters for electron versus hole CT are consistently found for all DFs employed. Our choice of the M06-2X/6-31G(d) recipe for the bulk of the rest of the paper rests on it lying between the two %HF exchange extremes and therefore the least compromised in terms of Δ BL energetics.[41] In short, the key observation is that $\lambda_e < \lambda_h$ for **H₂DP₂DPP** and that these values consistently scale with computed $\Sigma|\Delta$ BL| which in turn is dependent on the %HF in the DF employed.

3.2 Dependence of $\lambda_{h/e}$ on phenyl ring torsion relative to the DPP core in **H₂P₂DPP**

Several of the DPP derivatives we are interested in are substituted at R1 (Figure 1) in order to imbue solid state/thin film materials based on such DPPs with positive fluorescence properties.

TABLE 2 HERE

FIGURE 4 HERE

Substitution at R1 leads to the phenyl/DPP torsional angle(s) θ_1 and θ_2 deviating away from ca 7° (computed for neutral **H₂P₂DPP**) by as much as 35° (torsional angles defined in Figure 3). In contrast to similarly substituted T₂DPPs which remain essentially planar on R1 substitution, this results in significant phenyl/DPP core torsional angles in P₂DPPs. Therefore we examined the dependence of

$\lambda_{h/e}$ on 10° step-wise, simultaneous increases in θ_1 and θ_2 from 0 to 90° in **H₂P₂DPP** as well as the impact of these torsions on Δ BL. These were all M06-2X/6-31G(d) computed equilibrium geometries subject to the constraints imposed on θ_1 and θ_2 .

If the phenyl rings are rotated in such a way as to keep them parallel to one another then structures generally possessing C_i symmetry result and $\theta_1 = -\theta_2$ increments are used. On the other hand, if the phenyl rings are rotated in such a way as to lead to a crossing of the ring, then C_2 symmetry structures generally result. This would correspond to $\theta_1 = \theta_2$ step-wise increments. We will focus on the former $\theta_1 = -\theta_2$ incremental approach leading to C_i symmetric structures. We have looked at the C_2 series and small differences in $\lambda_{h/e}$ (of up to 4 kJ mol^{-1}) were obtained for any given C_2 structure relative to its associated C_i structure at equal θ constrains. However the overall trends observed within the two series were effectively the same. We will concentrate our discussion on the C_i series.

The results for the C_i series are tabulated in Table 2 together with those of fully relaxed, unconstrained **H₂P₂DPP** and **DPP** for comparison. Figure 4 illustrates the overall trends as discussed below. The most striking feature of the results is the greater response of λ_e to phenyl torsional twist than λ_h to such an extent that the relative ordering of λ_e and λ_h completely reverses at $\theta_1 = -\theta_2 = 60^\circ$; below 60° of twist $\lambda_e < \lambda_h$ whereas above 60° of twist $\lambda_e > \lambda_h$.

FIGURE 5 HERE

Figure 5 shows the effect of 90° DPP/phenyl torsion on the HOMOs and LUMOs of neutral **H₂P₂DPP**. it can be seen that in both cases all of the orbital density localises on the DPP core with progression from 0 to 90° of twist. In effect, the HOMO and LUMO densities of the 90° twisted structure are the same as those of the un-substituted parent, **DPP**. If $\lambda_{h/e}$ is dominated by Δ BL, as suggested previously, then $\lambda_{h/e}$ of **DPP** may be anticipated to demarcate the upper limits of $\lambda_{h/e}$ of the most twisted forms of **H₂P₂DPP** as both the hole (HOMO) and electron (LUMO) are effectively

confined to the DPP core. This indeed appears to be the case for λ_h but clearly not for λ_e (see Table 2 and Figure 4).

Variation of ΔBL with torsional twist for both CT processes was examined in more detail and the results summarised in Figure 6. Figures 6 A and B plot ΔBL s as a function of bond number along the long molecular axis of **H₂P₂DPP**. Figure 6A for $\theta_1 = -\theta_2 = 0^\circ$ and Figure 6B for $\theta_1 = -\theta_2 = 90^\circ$. Figures 6 C and D illustrate the same information for ΔBL along the short molecular axis of **H₂P₂DPP**. Figure 6 effectively summarises the contribution of each ΔBL in **H₂P₂DPP** to the overall structural reorganisation taking place on CT. ΔBL was computed by subtracting the bond length of a given bond of the neutral species from the bond length of the radical ion species for the same bond.

FIGURE 6 HERE

There are several striking features in Figure 6. The first is that the yellow oscillations of the radical cation ΔBL s are overall larger in amplitude than those of the blue of the radical anion across both molecular axes whether the geometry is completely planar or fully twisted. If ΔBL dominates structural reorganisation then it may be anticipated that $\lambda_e < \lambda_h$ for all degrees of twist. Indeed the larger computed values of λ_h than λ_e for both **DPP** as well as planar **H₂P₂DPP** are consistent with ΔBL dominating structural reorganisation in these instances.

The second feature, from Figures 6 A and B, is how little the effect of 90° torsion is on ΔBL for the long π -conjugated axis in both radical ions. The only significant ΔBL s apparent in both radical ions are the bond 2 and -2 that have a degree of anti- and bonding character in the HOMO and the LUMO respectively (see Figure 5). Removing an electron to create a hole results a decrease of anti-bonding character in bonds -2 and 2 while adding an electron to the LUMO creating the anion increases bonding character in these bonds; therefore ΔBL is negative in both cases. It can also be seen that the

Δ BL of the planar anion extends out in to the phenyl rings (bonds -1, 3 and 5) to a similar extent as the planar cation structure (bonds -5, -4, -3 and 3).

As the phenyl rings are twisted out of plane with respect to the DPP core, Δ BL for both radical ions is increasingly concentrated into the **DPP** core (Figure 6 C and D). Therefore, if Δ BL dominates structural reorganisation, then it is anticipated that $\lambda_{h/e}$ value of DPP should effectively mark the upper limits for those of the **H₂P₂DPP** twist series. This is borne out for the radical cation where λ_h values of 57.9 and 58.5 kJ mol⁻¹ are obtained for 90° twisted **H₂P₂DPP** and **DPP** respectively, but categorically fails for λ_e ; $\lambda_e = 73.0$ and 34.6 kJ mol⁻¹ for 90° twisted **H₂P₂DPP** and **DPP** respectively.

Clearly the presence of phenyl groups affects λ_e differently to λ_h as phenyl/DPP torsional angle increases in **H₂P₂DPP**. the large changes in λ_e observed must therefore arise from increasingly significant reorganisation processes other than Δ BL being present uniquely in the radical anion of **H₂P₂DPP** (with respect to the species in Table 2) at large degrees of twist ($\theta_1 = -\theta_2 > 30^\circ$).

FIGURE 7 HERE

All of the C and N core atoms in **DPP** are computed as lying in the same plane in the neutral and radical ions; out of plane bending modes associated with the DPP core therefore make little contribution to either λ_e or λ_h for **DPP**. A similar situation arises in the neutral and radical cation structures of **H₂P₂DPP** at $\theta_1 = -\theta_2 = 0$ and 90° of twist. It is expected therefore that Δ BL dominates $\lambda_{h/e}$ in these systems - which is consistent with the results associated with these species given in Table 2 and Figure 4.

However, the situation is different for the radical anion structures of **H₂P₂DPP** where out of plane deformations of the DPP core increase over the full range of torsional twist while the neutral species remains planar in this respect. The extent of the out of plane deformation in the radical anion can be quantified in terms of the sum of the three bond angles associated with the C7 (and C8) atoms of the

DPP core, $\Sigma\angle$ which will be 360° in a planar structure and less than 360° as pyramidalisation at the C7/8 locations increases. Figure 7 summarises the dependence of $\lambda_{h/e}$ on the differences in $\Sigma\angle$, $\Delta|\Sigma\angle|$ between radical ion and neutral species for **H₂P₂DPP** and also shows the neutral and 90° twisted structures of the radical anion superimposed on top of one another. In these structures the DPP core lies perpendicular to the plane of the diagram. It is seen that the relative angles of the phenyl groups (lying in the plane of the diagram) reflect increased pyramidalisation of the C7/8 atoms in the radical anion versus neutral species at 90° of phenyl twist. The plot of λ_e versus $\Delta|\Sigma\angle|$ is linear whereas that of λ_h shows a negligible correlation with $\Delta|\Sigma\angle|$.

Figure 7 suggests that the reason λ_e of **H₂P₂DPP** is greater than that of **DPP** at $\theta > 30^\circ$ of twist is the contribution from out of plane bending modes to λ_e in the highly twisted phenyl substituted species which are absent in **DPP**. It can be seen (Table 2) that λ_e^{NR} becomes greater than λ_e^{RN} as θ increases – indicating that the frequency of the key reorganizational contribution of the out of plane bending modes(s) is (are) greater for the neutral than radical anion species. This can be accounted for as follows: the HOMO of **H₂P₂DPP** in Figure 5 shows that such deformation is associated with disruption of bonding interactions in bonds 1 and -1 in the neutral species, but anti-bonding in the LUMO that becomes singly occupied in the anion radical species. It is therefore anticipated that the force constants of such out of plane vibrations are greater for neutral than they are for radical anion species leading in turn to a decrease in the vibrational frequency of the bending mode in the radical anion relative to neutral form. Thus the PES associated with CT progression from neutral to radical anion twisted geometries is steeper than that for the radical anion to neutral twisted geometry and λ_e^{NR} is greater than λ_e^{RN} .

FIGURE 8 HERE

The driving force for these out of plane deformed, 90° twisted anionic **H₂P₂DPP** structures is likely the presence of a strong intra-molecular electrostatic interactions between the DPP core carbonylic

oxygen and the closest ortho hydrogen as illustrated by the valence type structure in Figure 8. A clear correlation between $\Delta|\Sigma\langle|$ and the difference in O \cdots H distance between radical anion and neutral geometries, $\Delta|O\cdots H|$ is observed as given by Figure 8. The O \cdots H distance becomes increasingly less in the radical anion than neutral structures as θ increases and maintaining these shorter distances requires ever greater out of plane bending of the DPP core.

The key findings in this section are therefore as follows; i) at low degrees of phenyl/torsional twist $\lambda_e < \lambda_h$, ii) increasing torsional twist leads to λ_e increasing far more rapidly than λ_h such that their relative ordering crosses at $\theta_1 = -\theta_2 = 60^\circ$ beyond which $\lambda_e > \lambda_h$, iii) increases in λ_h of **H₂P₂DPP** with phenyl twist are consistent with increased charge localisation on the DPP core and therefore larger amplitude changes in Δ BL of the radical cation. The λ_h of **DPP** therefore effectively gives the upper limit of λ_h for **H₂P₂DPP** at large twist angles. This Δ BL amplitude dependence on torsional twist will also affect λ_e ; λ_e for DPP is 34.5 kJ mol⁻¹, iv) however the main driver of the increases in λ_e with θ for **H₂P₂DPP** is out of plane bending of the central DPP core in order to facilitate favourable electrostatic interaction between the O atoms of the core and the nearest H atoms of the phenyl rings and v) the larger force constant associated with out of plane bending of the neutral species than the radical anion results in the growing inequality between λ_e^{NR} and λ_e^{RN} as θ increases.

3.3 Effects on $\lambda_{h/e}$ of methyl substitution at R1 and replacing phenyl with thiophenyl rings

The out of plane bending contributions to λ_e with increasing θ in **H₂P₂DPP** are driven to an extent by imposing constrains on θ_1 and θ_2 . Similar constrains may arise in chemical/physical environments such as crystalline or inert matrices which restrict torsional motion. However, in less ordered environments such as amorphous thin films or polymers, it is quite possible torsional motion about θ_1 (and θ_2) is hindered less by the immediate environment surrounding the DPP.

TABLE 3 HERE

We compute $\theta_1 = -\theta_2 = 28.2^\circ$ in fully relaxed neutral **Me₂P₂DPP** versus 7.7° in **H₂P₂DPP**. In both cases torsional relaxation occurs in this coordinate on formation of radical ion species although consistently to a greater extent in the radical anion versus radical cation. Changes in θ on forming radical cation and anion, $\Delta\theta_C$ and $\Delta\theta_A$ respectively are listed in Table 3 along with the relevant contributions to $\lambda_{h/e}$. We have also computed $\lambda_{h/e}$ for two thiophenyl substituted DPPs; **H₂T₂DPP** and **Me₂T₂DPP**. These latter systems approach full planarity in their neutral and both radical ion forms. Table 3 includes $\lambda_{h/e}$ values of these species along with those of anthracene, **anthr**, and pentacene, **pent** for comparison. First we discuss those of the linear acenes.

The $\lambda_{h/e}$ values for **anthr** and **pent** in Table 3 were determined using M06-2X/6-31G(d) and for comparison B3LYP/6-31G(d) (listed in Table 3 in italics). The differences between B3LYP and M06-2X values can be accounted for on the basis of Δ BL dominating $\lambda_{h/e}$ in these systems. As expected based on Figure 2, it can be seen that the B3LYP $\lambda_{h/e}$ values are lower (by 5-7 kJ mol⁻¹) than those obtained using M06-2X. The B3LYP results agree within 1 kJ mol⁻¹ of the published values (often employing larger basis sets).[38, 54, 55]

Turning to the DPPs, once again we find that $\lambda_e < \lambda_h$ for all of the DPPs in Table 3 irrespective of **H/Me** and **P/T** group substitution. This relative ordering of $\lambda_e < \lambda_h$ at low θ values would seem to be an inherent property of the DPP core motif itself. Perhaps surprisingly there is little difference in $\lambda_{h/e}$ of **H₂P₂DPP**, **H₂T₂DPP** and **Me₂T₂DPP** suggesting that co-planarity of the various conjugated rings is more significant than the nature of the rings themselves.

The outlier within this DPP series is **Me₂P₂DPP**. Here the neutral structure is non-planar ($\theta_1 = -\theta_2 = 28.2^\circ$) and significant changes towards co-planarity occur on formation of the radical anion ($\Delta\theta_A = 10.6^\circ$) but not the radical cation ($\Delta\theta_C = 0.9^\circ$). This can be explained by the bonding interactions of the singly occupied LUMO at positions -2 and 2 in the long axis of phenyl substituted DPPs (see Figure 5) enhancing resonance stabilisation of the radical species with increasing co-planarity of the three ring systems. This same bonding interaction leads to a steeper PES for twisting the anion out of plane than for the neutral species where the HOMO is anti-bonding in character at these bond positions. The

differing curvatures of the neutral and radical anion PESs along the torsional CT coordinate is responsible for the slightly larger λ_e^{RN} than λ_e^{NR} value in Table 3. Note that this is the opposite of their relative contributions to λ_e when θ is constrained to a fixed degree of twist as examined previously. The 10° torsional relaxation of **Me₂P₂DPP** on radical anion formation results in larger λ_e of 34 versus 20-24 kJ mol⁻¹ found for more planar DPP structures whereas all of the DPP λ_h values are similar (47.6 ± 2.0 kJ mol⁻¹) reflecting the small degree of torsional relaxation all of the radical cations experience (including that of **Me₂P₂DPP**).

These results echo those listed in Table 2 and illustrated in Figure 4; for all the DPPs examined λ_e is far more sensitive to twist about θ_1 and θ_2 than λ_h , whether or not these torsional angles are constrained. It is likely that the O...H atoms intra-molecular electrostatic interactions illustrated in Figure 8 are responsible for this sensitivity of λ_e as bending out of plane (for fixed torsions) and torsional relaxation (in unconstrained, non-planar DPP systems) both lead to a decrease in the O...H distances in the radical anion.

For all DPPs in Table 3, we find that $|\Delta\Sigma|$ is effectively 0° suggesting that out of plane bending contributions to $\lambda_{h/e}$ are negligible as anticipated by Figure 5 for low values of θ . The main contributor to $\lambda_{h/e}$ values in planar **P** or **T** substituted DPPs is therefore likely to be high frequency C-C stretching modes through their contribution to ΔBL . A combination of high frequency C-C modes and low frequency torsional modes will contribute to λ_e to a greater extent than λ_h in non-planar **P** and **T** substituted DPP systems with out of plane bending modes contributing further to λ_e at larger and more constrained degrees of torsional twist.

Given the characteristic $\lambda_e < \lambda_h$ for all of the DPPs listed in Table 3, it is interesting to determine how these values translate with relative rate constants for electron, k_e versus hole, k_h CT using Equation 1. Ratios of $k_e/k_h = 6.1$ and 20.3 for **Me₂P₂DPP** and **Me₂T₂DPP** respectively are obtained using the data in Table 3 assuming identical values for V for electron and hole transfer. Crude as these calculations are, they point to DPPs, based around the structures in Table 3, inherently favouring electron over hole CT processes by an order of magnitude or so.

Electron transfer processes in DPP based organic electronic devices such as OFETs are inherently more susceptible to quenching by impurities (O_2 and H_2O in particular) and annealing treatments than are hole transfer processes.[8] The mobility of both CT carriers may also be influenced by device architecture so comparison of such crudely estimated electron versus hole transfer rate constants with experimentally observed charge mobility is fraught. Nevertheless, there is one particular report of OFET devices based on **R₂T₂DPP** type dimer structures which in one configuration demonstrates a field effect electron mobility of up to $3 \text{ cm}^2 \text{ V}^{-1} \text{ s}^{-1}$ and negligible hole mobility.[13] Upon changing device configuration, an ambipolar field effect charge mobility was observed with hole and electron mobilities of around $0.1 \text{ cm}^2 \text{ V}^{-1} \text{ s}^{-1}$ reported. There are also reports of ambipolar charge mobility in DPP based OFETs slightly favouring electron over hole transport processes by a factor of 1 – 2,[6, 7, 10-12] although the DPP structures employed are often far more complex than those modelled here. Over and beyond device architecture and impurities, of course we are ignoring the role of V in these device systems as well as our own. The key point we make is that there are reports of enhanced, if not competitive electron versus hole mobility in OFET devices based on DPP materials which, given the greater susceptibility of electron transport quenching over hole, may well reflect $\lambda_e < \lambda_h$ we report here.

4. Conclusions

We summarise our main findings as follows; i) $\lambda_e < \lambda_h$ for phenyl and thiophenyl substituted DPPs, ii) λ_e is far more sensitive to torsional twist of the phenyl rings with respect to the DPP core than λ_h and at very large torsional angles ($> 60^\circ$) the ordering switches such that $\lambda_e > \lambda_h$ and iii) alkyl substitution at the N atoms of the DPP core increases λ_e for diphenyl DPP derivatives relative to thiophenyl substitution because significant torsional relaxation contributes to the reorganisation energy in the former but not the latter species. On the other hand, λ_h is not significantly different in these two systems.

Taken together these findings suggest that electron transport in organic devices based on **P₂/T₂DPP** derivatives is inherently favoured by up to an order of magnitude (or thereabouts) over hole transport

for the same degree of electronic coupling but at the same time will be far more sensitive to environmental influence on co-planarity of the rings systems than hole transfer. Alkyl substitution of the DPP core N atoms confers ease of solubility on these materials and so thiophenyl are a better choice (due to co-planarity with the DPP core) to maximise electron transport rate than phenyl derivatives although little difference in hole transport between the two substituents is expected. Current strategies employing DPPs in OFET design are overwhelmingly based around thiophenyl substitution and several recent results are consistent with our findings; greater electron charge mobility over hole,[13] ambipolar properties[6, 7, 10-12] and device annealing[8] (thereby altering physical environment surrounding the DPP) affecting electron transport to a greater extent than hole transport.

On the other hand, we find that alkylation of **P₂DPPs** generally results in effective fluorescent thin film and crystalline materials unlike **T₂DPPs**. This opens up the potential for novel charge/light environmental response materials based on phenyl substitution which we hope to develop and report in the near future.

Acknowledgements

CJM acknowledge EPSRC for funding under the First Grant Scheme EP/J011746/1, AJM acknowledges PhD funding for JCC from UWS.

References

- [1] Hao ZM, Iqbal A. Some aspects of organic pigments. *Chem Soc Rev.* 1997;26(3):203-13.
- [2] Wallquist O, Lenz R. 20 years of DPP Pigments - Future perspectives. *Macromolecular Symposia.* 2002;187:617-29.
- [3] Christie RM. *Colour Chemistry: The Royal Society of Chemistry*, 2001.
- [4] Herbst W, Hunger K. *Industrial Organic Pigments: Wiley-VCH*, 2004.
- [5] Smith HM. *High Performance Pigments: Wiley-VCH*, 2002.
- [6] Hong W, Sun B, Aziz H, Park W-T, Noh Y-Y, Li Y. A conjugated polyazine containing diketopyrrolopyrrole for ambipolar organic thin film transistors. *Chem Commun.* 2012;48(67):8413-5.

- [7] Lee J, Cho S, Seo JH, Anant P, Jacob J, Yang C. Swapping field-effect transistor characteristics in polymeric diketopyrrolopyrrole semiconductors: debut of an electron dominant transporting polymer. *J Mater Chem*. 2012;22(4):1504-10.
- [8] Chen Z, Lee MJ, Ashraf RS, Gu Y, Albert-Seifried S, Nielsen MM, et al. High-Performance Ambipolar Diketopyrrolopyrrole-Thieno 3,2-b thiophene Copolymer Field-Effect Transistors with Balanced Hole and Electron Mobilities. *Adv Mater*. 2012;24(5):647-+.
- [9] Cortizo-Lacalle D, Arumugam S, Elmasly SET, Kanibolotsky AL, Findlay NJ, Inigo AR, et al. Incorporation of fused tetrathiafulvalene units in a DPP-terthiophene copolymer for air stable solution processable organic field effect transistors. *J Mater Chem*. 2012;22(22):11310-5.
- [10] Ha JS, Kim KH, Choi DH. 2,5-Bis(2-octyldodecyl)pyrrolo 3,4-c pyrrole-1,4-(2H,5H)-dione-Based Donor-Acceptor Alternating Copolymer Bearing 5,5'-Di (thiophen-2-yl)-2,2'-biselenophene Exhibiting $1.5 \text{ cm}^2 \cdot \text{V}^{-1} \cdot \text{s}^{-1}$ Hole Mobility in Thin-Film Transistors. *J Am Chem Soc*. 2011;133(27):10364-7.
- [11] Sonar P, Singh SP, Li Y, Soh MS, Dodabalapur A. A Low-Bandgap Diketopyrrolopyrrole-Benzothiadiazole-Based Copolymer for High-Mobility Ambipolar Organic Thin-Film Transistors. *Adv Mater*. 2010;22(47):5409-+.
- [12] Bronstein H, Chen Z, Ashraf RS, Zhang W, Du J, Durrant JR, et al. Thieno 3,2-b thiophene-Diketopyrrolopyrrole-Containing Polymers for High-Performance Organic Field-Effect Transistors and Organic Photovoltaic Devices. *J Am Chem Soc*. 2011;133(10):3272-5.
- [13] Kanimozhi C, Yaacobi-Gross N, Chou KW, Amassian A, Anthopoulos TD, Patil S. Diketopyrrolopyrrole-Diketopyrrolopyrrole-Based Conjugated Copolymer for High-Mobility Organic Field-Effect Transistors. *J Am Chem Soc*. 2012;134(40):16532-5.
- [14] Qu S, Tian H. Diketopyrrolopyrrole (DPP)-based materials for organic photovoltaics. *Chem Commun*. 2012;48(25):3039-51.
- [15] Holcombe TW, Yum J-H, Yoon J, Gao P, Marszalek M, Di Censo D, et al. A structural study of DPP-based sensitizers for DSC applications. *Chem Commun*. 2012;48(87):10724-6.
- [16] Qu S, Qin C, Islam A, Wu Y, Zhu W, Hua J, et al. A novel D-A-pi-A organic sensitizer containing a diketopyrrolopyrrole unit with a branched alkyl chain for highly efficient and stable dye-sensitized solar cells. *Chem Commun*. 2012;48(55):6972-4.
- [17] Qu S, Wu W, Hua J, Kong C, Long Y, Tian H. New Diketopyrrolopyrrole (DPP) Dyes for Efficient Dye-Sensitized Solar Cells. *J Phys Chem C*. 2010;114(2):1343-9.
- [18] Yum J-H, Holcombe TW, Kim Y, Yoon J, Rakstys K, Nazeeruddin MK, et al. Towards high-performance DPP-based sensitizers for DSC applications. *Chem Commun*. 2012;48(87):10727-9.

- [19] Kanimozhi C, Balraju P, Sharma GD, Patil S. Diketopyrrolopyrrole-Based Donor-Acceptor Copolymers as Organic Sensitizers for Dye Sensitized Solar Cells. *J Phys Chem C*. 2010;114(7):3287-91.
- [20] Loser S, Bruns CJ, Miyauchi H, Ortiz RP, Facchetti A, Stupp SI, et al. A Naphthodithiophene-Diketopyrrolopyrrole Donor Molecule for Efficient Solution-Processed Solar Cells. *J Am Chem Soc*. 2011;133(21):8142-5.
- [21] Tamayo AB, Walker B, Nguyen T-Q. A low band gap, solution processable oligothiophene with a diketopyrrolopyrrole core for use in organic solar cells. *J Phys Chem C*. 2008;112(30):11545-51.
- [22] Tamayo AB, Dang X-D, Walker B, Seo J, Kent T, Nguyen T-Q. A low band gap, solution processable oligothiophene with a dialkylated diketopyrrolopyrrole chromophore for use in bulk heterojunction solar cells. *Appl Phys Lett*. 2009;94(10).
- [23] Bredas JL, Beljonne D, Coropceanu V, Cornil J. Charge-transfer and energy-transfer processes in pi-conjugated oligomers and polymers: A molecular picture. *Chem Rev*. 2004;104(11):4971-5003.
- [24] Marcus RA. ELECTRON-TRANSFER REACTIONS IN CHEMISTRY - THEORY AND EXPERIMENT. *Reviews of Modern Physics*. 1993;65(3):599-610.
- [25] Marcus RA, Sutin N. ELECTRON TRANSFERS IN CHEMISTRY AND BIOLOGY. *Biochimica Et Biophysica Acta*. 1985;811(3):265-322.
- [26] Bixon M, Jortner J. Electron transfer - From isolated molecules to biomolecules. In: Jortner J, Bixon M, editors. *Electron Transfer-from Isolated Molecules to Biomolecules*, Pt 11999. p. 35-202.
- [27] Matyushov DV. Solvent reorganization energy of electron-transfer reactions in polar solvents. *J Chem Phys*. 2004;120(16):7532-56.
- [28] McMahon DP, Troisi A. Evaluation of the External Reorganization Energy of Polyacenes. *J Phys Chem Lett*. 2010;1(6):941-6.
- [29] Vath P, Zimmt MB. A spectroscopic study of solvent reorganization energy: Dependence on temperature, charge transfer distance, and the type of solute-solvent interactions. *J Phys Chem A*. 2000;104(12):2626-33.
- [30] Li XY, Tong J, He FC. Ab initio calculation for inner reorganization energy of gasphase electron transfer in organic molecule-ion systems. *Chem Phys*. 2000;260(3):283-94.
- [31] Bromley ST, Illas F, Mas-Torrent M. Dependence of charge transfer reorganization energy on carrier localisation in organic molecular crystals. *Phys Chem Chem Phys*. 2008;10(1):121-7.
- [32] Zade SS, Bendikov M. Study of hopping transport in long oligothiophenes and oligoselenophenes: Dependence of reorganization energy on chain length. *Chem Eur J*. 2008;14(22):6734-41.

- [33] Sakanoue K, Motoda M, Sugimoto M, Sakaki S. A molecular orbital study on the hole transport property of organic amine compounds. *J Phys Chem A*. 1999;103(28):5551-6.
- [34] Lin BC, Cheng CP, Lao ZPM. Reorganization energies in the transports of holes and electrons in organic amines in organic electroluminescence studied by density functional theory. *J Phys Chem A*. 2003;107(26):5241-51.
- [35] Coropceanu V, Andre JM, Malagoli M, Bredas JL. The role of vibronic interactions on intramolecular and intermolecular electron transfer in pi-conjugated oligomers. *Theor Chem Acc*. 2003;110(2):59-69.
- [36] Malagoli M, Bredas JL. Density functional theory study of the geometric structure and energetics of triphenylamine-based hole-transporting molecules. *Chem Phys Lett*. 2000;327(1-2):13-7.
- [37] Reimers JR. A practical method for the use of curvilinear coordinates in calculations of normal-mode-projected displacements and Duschinsky rotation matrices for large molecules. *J Chem Phys*. 2001;115(20):9103-9.
- [38] Gruhn NE, da Silva DA, Bill TG, Malagoli M, Coropceanu V, Kahn A, et al. The vibrational reorganization energy in pentacene: Molecular influences on charge transport. *J Am Chem Soc*. 2002;124(27):7918-9.
- [39] Malagoli M, Coropceanu V, da Silva DA, Bredas JL. A multimode analysis of the gas-phase photoelectron spectra in oligoacenes. *J Chem Phys*. 2004;120(16):7490-6.
- [40] Coropceanu V, Malagoli M, da Silva DA, Gruhn NE, Bill TG, Bredas JL. Hole- and electron-vibrational couplings in oligoacene crystals: Intramolecular contributions. *Phys Rev Lett*. 2002;89(27).
- [41] Zhao Y, Truhlar DG. The M06 suite of density functionals for main group thermochemistry, thermochemical kinetics, noncovalent interactions, excited states, and transition elements: two new functionals and systematic testing of four M06-class functionals and 12 other functionals. *Theor Chem Acc*. 2008;120(1-3):215-41.
- [42] Szabo A, Ostlund NS. *Modern Quantum Chemistry: Introduction to Advanced Electronic Structure Theory*: McGraw-Hill, 1989.
- [43] Jensen F. *Introduction to computational chemistry*: John Wiley and sons, 2007.
- [44] Leach AR. *Molecular Modelling. Principles and applications*: Prentice-Hall, 2001.
- [45] Coropceanu V, Cornil J, da Silva Filho DA, Olivier Y, Silbey R, Bredas J-L. Charge transport in organic semiconductors. *Chem Rev*. 2007;107(4):926-52.
- [46] Becke AD. DENSITY-FUNCTIONAL THERMOCHEMISTRY .3. THE ROLE OF EXACT EXCHANGE. *J Chem Phys*. 1993;98(7):5648-52.

- [47] Becke AD. DENSITY-FUNCTIONAL EXCHANGE-ENERGY APPROXIMATION WITH CORRECT ASYMPTOTIC-BEHAVIOR. *Physical Review A*. 1988;38(6):3098-100.
- [48] Lee CT, Yang WT, Parr RG. DEVELOPMENT OF THE COLLE-SALVETTI CORRELATION-ENERGY FORMULA INTO A FUNCTIONAL OF THE ELECTRON-DENSITY. *Physical Review B*. 1988;37(2):785-9.
- [49] Zhao Y, Truhlar DG. A new local density functional for main-group thermochemistry, transition metal bonding, thermochemical kinetics, and noncovalent interactions. *J Chem Phys*. 2006;125(19).
- [50] Zhao Y, Truhlar DG. Density functional for spectroscopy: No long-range self-interaction error, good performance for Rydberg and charge-transfer states, and better performance on average than B3LYP for ground states. *J Phys Chem A*. 2006;110(49):13126-30.
- [51] Shao Y, Molnar LF, Jung Y, Kussmann J, Ochsenfeld C, Brown ST, et al. Advances in methods and algorithms in a modern quantum chemistry program package. *Phys Chem Chem Phys*. 2006;8(27):3172-91.
- [52] Filho DAdS, Coropceanu V, Fichou D, Gruhn NE, Bill TG, Gierschner J, et al. Hole-vibronic coupling in oligothiophenes: impact of backbone torsional. exibility on relaxation energies. *Philosophical Transactions of the Royal Society a-Mathematical Physical and Engineering Sciences*. 2007;365(1855):1435-52.
- [53] Zhao Y, Truhlar DG. Density functionals with broad applicability in chemistry. *Acc Chem Res*. 2008;41(2):157-67.
- [54] Wang L, Nan G, Yang X, Peng Q, Li Q, Shuai Z. Computational methods for design of organic materials with high charge mobility. *Chem Soc Rev*. 2010;39(2):423-34.
- [55] Kuo M-Y, Chen H-Y, Chao I. Cyanation: Providing a three-in-one advantage for the design of n-type organic field-effect transistors. *Chem Eur J*. 2007;13(17):4750-8.

Captions

Table 1. Computed reorganization energies in kJ mol^{-1} for hole and electron charge transfer processes for **H₂P₂DPP** using different DFs at 6-31G(d) level. All results in brackets for constrained geometries, $\theta_1 = -\theta_2 = 0^\circ$

Table 2 Computed $\lambda_{h/e}$ values in kJ mol^{-1} for **H₂P₂DPP** as a function of phenyl ring torsion. M06-2X/6-31G(d)//M06-2X/6-31G(d)

Table 3 Comparison of $\lambda_{h/e}$ and $\Delta\theta_{C/A}$ for several DPP-based molecular systems. M06-2X/6-31G(d)//M06-2X/6-31G(d). Values in *italics* denote calculations performed using B3LYP/6-31G(d)//B3LYP/6-31G(d). Anthracene (**anthr**) and Pentacene (**pent**) included for comparison.

Figure 1 Structures of the different DPP-based systems examined

Figure 2 Dependence of λ_h (yellow filled circles) and λ_e (blue filled circles) on percentage of Hartree-Fock exchange utilised by the density functional for the constrained series listed in Table 1. DF/6-31G(d)//DF/6-31G(d). $\theta_1 = -\theta_2 = 0^\circ$.

Figure 3 Sum of the absolute bond length changes between radical ion and neutral **H₂P₂DPP** as a function of % Hartree-Fock exchange in the DF. Ordering of DFs from left to right as per Figure 2. DF/6-31G(d)//DF/6-31G(d). $\theta_1 = -\theta_2 = 0^\circ$.

Figure 4 Plot of hole (yellow filled circles) and electron (blue filled circles) CT reorganisation energies, $\lambda_{h/e}$ of constrained **H₂P₂DPP** as a function of phenyl ring torsion about θ . θ_1 and θ_2 are defined by red stars on the **H₂P₂DPP** structure. $\lambda_{h/e}$ are illustrated by transparent circles on the $\lambda_{h/e}$ axis. M06-2X/6-31G(d)//M06-2X/6-31G(d).

Figure 5 Highest occupied and lowest unoccupied molecular orbitals (HOMO and LUMO respectively) of neutral **H₂P₂DPP** constrained at 0 and 90° . M06-2X/6-31G(d). IsoVal = 0.02

Figure 6 Plot of the difference in bond length, ΔBL between constrained C_i structures of radical cation (yellow filled circles) and radical anion (blue filled circles) and the parent neutral **H₂P₂DPP** versus bond number over the molecular axis as indicated by inserted structures. A and C; $\theta_1 = -\theta_2 = 0^\circ$. B and D $\theta_1 = -\theta_2 = 90^\circ$. M06-2X/6-31G(d)//M06-2X/6-31G(d).

Figure 7 Plot of $\lambda_{h/e}$ as a function of the difference in the sum of C7 bond angle between radical anion (blue filled circles) and radical cation (yellow filled circles) and the neutral form for **H₂P₂DPP**. M06-2X/6-31G(d)//M06-2X/6-31G(d). Inset depicts the neutral and radical anion (highlighted) optimized geometries for $\theta_1 = -\theta_2 = 90^\circ$.

Figure 8 Plot of the difference in the sum of C7 bond angles between radical ion and neutral **H₂P₂DPP** versus O···H distance. Blue; radical anion, yellow; radical cation. Inset: structure of radical anion. The dots in anion structure are centred on the C7 atoms. M06-2X/6-31G(d)//M06-2X/6-31G(d).

Table 1. Computed reorganization energies in kJ mol^{-1} for hole and electron charge transfer processes for **H₂P₂DPP** using different DFs at 6-31G(d) level. All results in brackets for constrained geometries, $\theta_1 = -\theta_2 = 0^\circ$

DF	%HF	$\lambda^{\text{NR}}_{\text{h}}$	$\lambda^{\text{RN}}_{\text{h}}$	λ_{h}	$\lambda^{\text{NR}}_{\text{e}}$	$\lambda^{\text{RN}}_{\text{e}}$	λ_{e}
M06-L	0	11.8 (11.9)	12.1 (12.1)	23.9 (24.0)	7.6 (8.0)	7.9 (7.7)	15.5 (15.8)
B3LYP	20	15.2 (14.2)	16.4 (16.1)	31.7 (30.3)	8.5 (9.1)	10.1 (9.4)	18.6 (18.5)
M06	27	16.5 (16.7)	17.4 (16.9)	33.9 (33.5)	9.2 (9.4)	10.2 (9.5)	19.4 (18.9)
M06-2X	54	22.5 (22.8)	23.2 (22.7)	45.8 (45.4)	11.5 (11.3)	12.3 (11.8)	23.8 (23.1)
M06-HF	100	33.3 (33.0)	34.0 (33.7)	67.3 (66.7)	14.8 (14.5)	14.9 (14.5)	29.6 (29.1)

Table 2 Computed $\lambda_{h/e}$ values in kJ mol^{-1} for **H₂P₂DPP** as a function of phenyl ring torsion.

M06-2X/6-31G(d)//M06-2X/6-31G(d)

$\theta_1 = -\theta_2 / ^\circ$	$\lambda_{\text{h}}^{\text{NR}}$	$\lambda_{\text{h}}^{\text{RN}}$	λ_{h}	$\lambda_{\text{e}}^{\text{NR}}$	$\lambda_{\text{e}}^{\text{RN}}$	λ_{e}
0	22.8	22.7	45.4	11.3	11.8	23.1
10	22.2	23.0	45.2	11.5	12.2	23.7
20	21.8	23.3	45.1	12.1	14.0	26.0
30	21.8	23.8	45.6	14.1	15.9	30.0
40	22.2	24.3	46.5	17.1	19.1	36.1
50	23.0	25.1	48.1	21.3	22.4	43.6
60	24.4	26.1	50.5	26.5	25.8	52.3
70	26.3	27.3	53.7	32.2	29.7	61.9
80	27.9	28.1	56.0	39.2	32.7	71.9
90	29.4	28.5	57.9	45.5	27.5	73.0
DPP	30.0	28.5	58.5	17.8	16.7	34.5
H₂P₂DPP	22.5	23.2	45.8	11.5	12.3	23.8

Table 3 Comparison of $\lambda_{h/e}$ and $\Delta\theta_{C/A}$ for several DPP-based molecular systems. M06-2X/6-31G(d)//M06-2X/6-31G(d). Values in *italics* denote calculations performed using B3LYP/6-31G(d)//B3LYP/6-31G(d). Anthracene (**anthr**) and Pentacene (**pent**) included for comparison.

Compound	$\Delta\theta_C$	$\Delta\theta_A$	λ_{h}^{NR}	λ_{h}^{RN}	λ_h	λ_e^{NR}	λ_e^{RN}	λ_e
anthr			10.7	9.8	20.5	13.1	12.3	25.4
			<i>7.6</i>	<i>6.7</i>	<i>14.3</i>	<i>10.5</i>	<i>9.7</i>	<i>20.2</i>
pent			7.5	7.7	15.2	9.0	9.2	18.2
			<i>4.2</i>	<i>3.9</i>	<i>8.1</i>	<i>6.0</i>	<i>6.8</i>	<i>12.8</i>
H₂P₂DPP	3.7	6.0	22.5	23.2	45.8	11.5	12.3	23.8
H₂T₂DPP	0.7	0.3	22.5	23.1	45.6	10.7	10.8	21.5
Me₂P₂DPP	0.9	10.6	24.5	25.1	49.6	15.7	18.2	33.9
Me₂T₂DPP	0.9	0.9	22.6	23.5	46.1	10.3	10.4	20.7
DPP			30.0	28.5	58.4	17.8	16.7	34.5

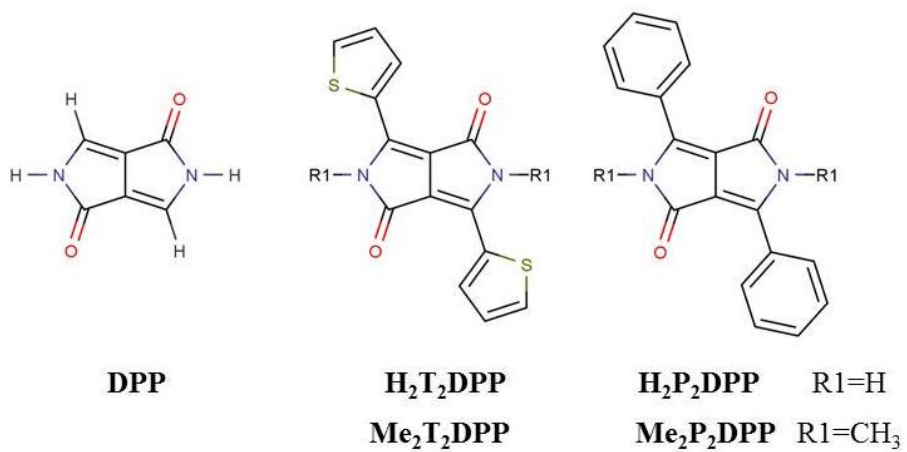


Figure 1 Structures of the different DPP-based systems examined

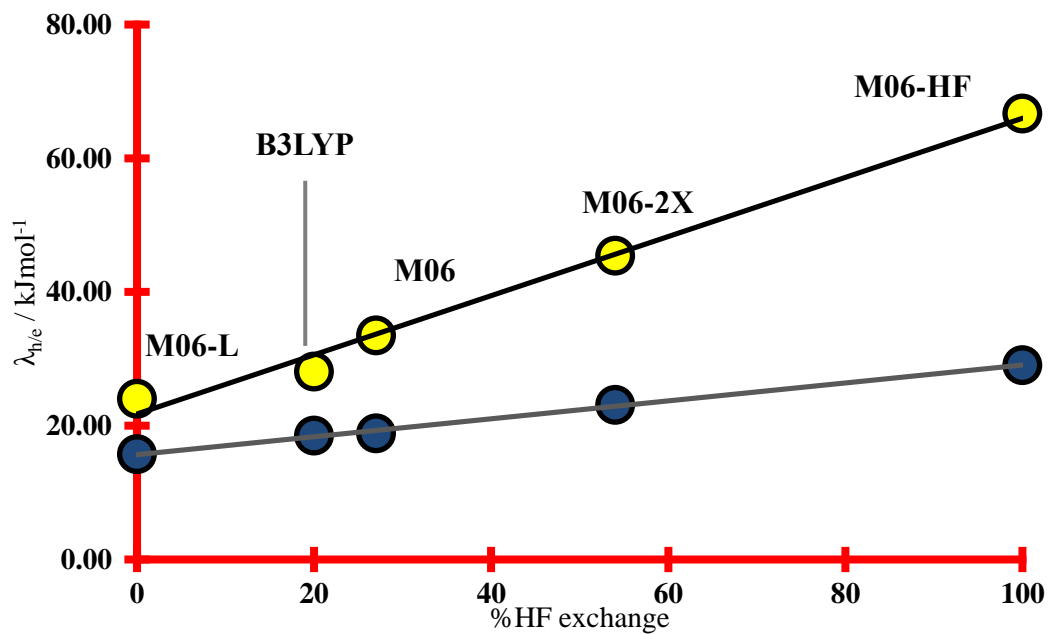


Figure 2 Dependence of λ_h (yellow filled circles) and λ_e (blue filled circles) on percentage of Hartree-Fock exchange utilised by the density functional for the constrained series listed in Table 1.

DF/6-31G(d)//DF/6-31G(d). $\theta_1 = -\theta_2 = 0^\circ$.

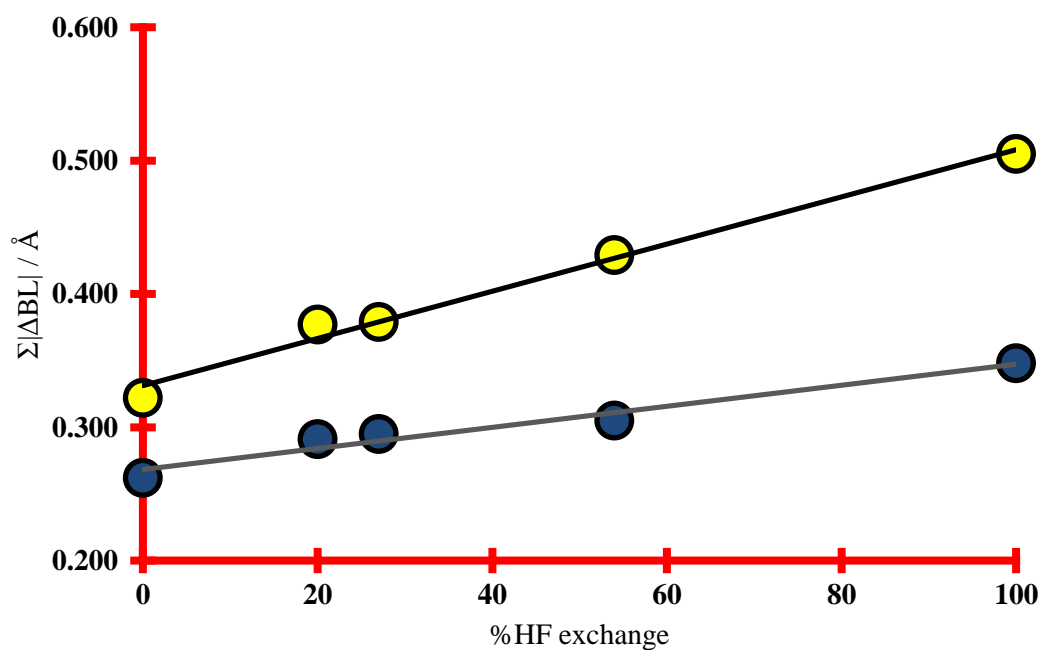


Figure 3 Sum of the absolute bond length changes between radical ion and neutral $\text{H}_2\text{P}_2\text{DPP}$ as a function of % Hartree-Fock exchange in the DF. Ordering of DFs from left to right as per Figure 2. DF/6-31G(d)//DF/6-31G(d). $\theta_1 = -\theta_2 = 0^\circ$.

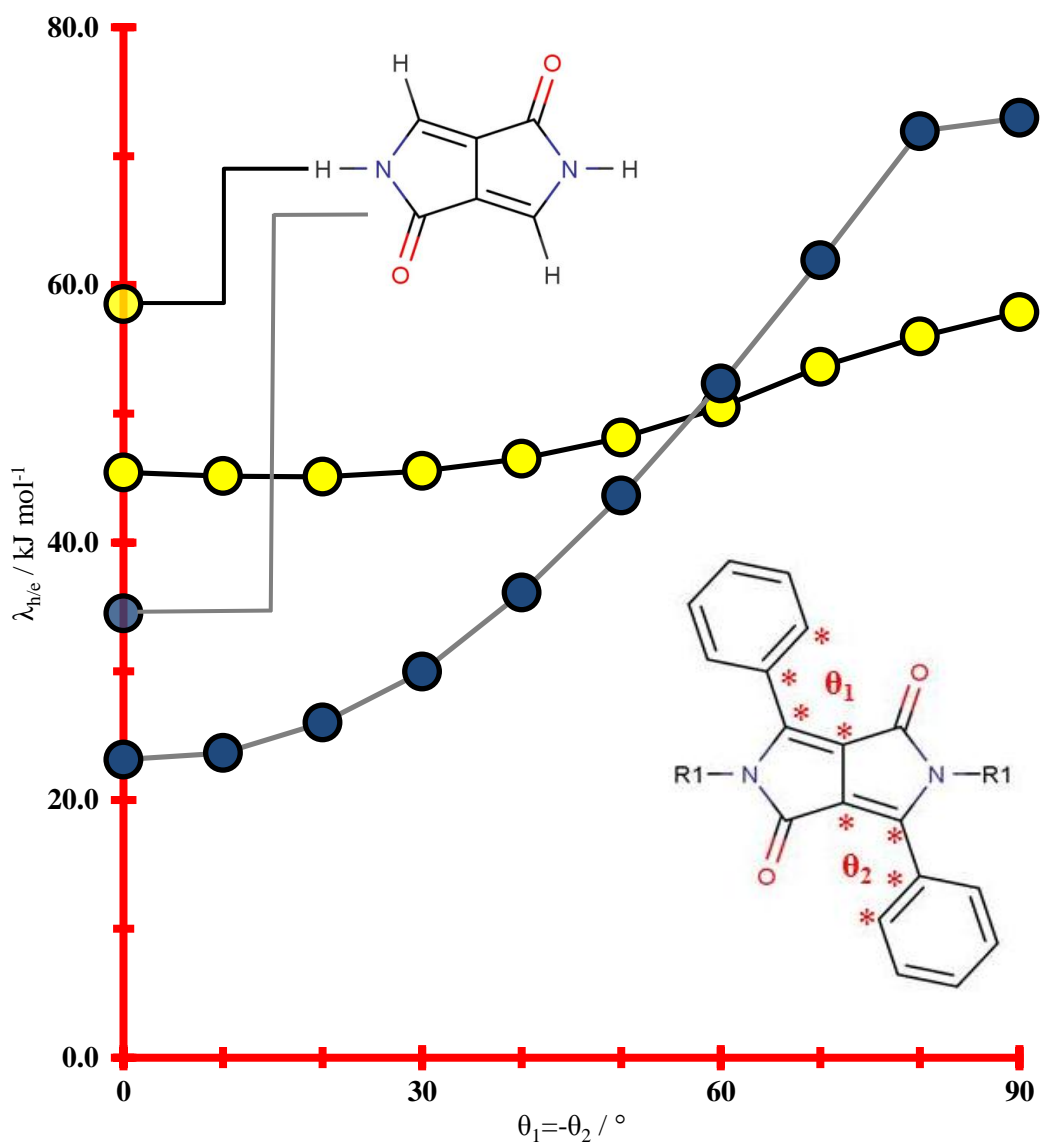


Figure 4 Plot of hole (yellow filled circles) and electron (blue filled circles) CT reorganisation energies, $\lambda_{h/e}$ of constrained $\text{H}_2\text{P}_2\text{DPP}$ as a function of phenyl ring torsion about θ . θ_1 and θ_2 are defined by red stars on the $\text{H}_2\text{P}_2\text{DPP}$ structure. $\lambda_{h/e}$ are illustrated by transparent circles on the $\lambda_{h/e}$ axis. M06-2X/6-31G(d)//M06-2X/6-31G(d).

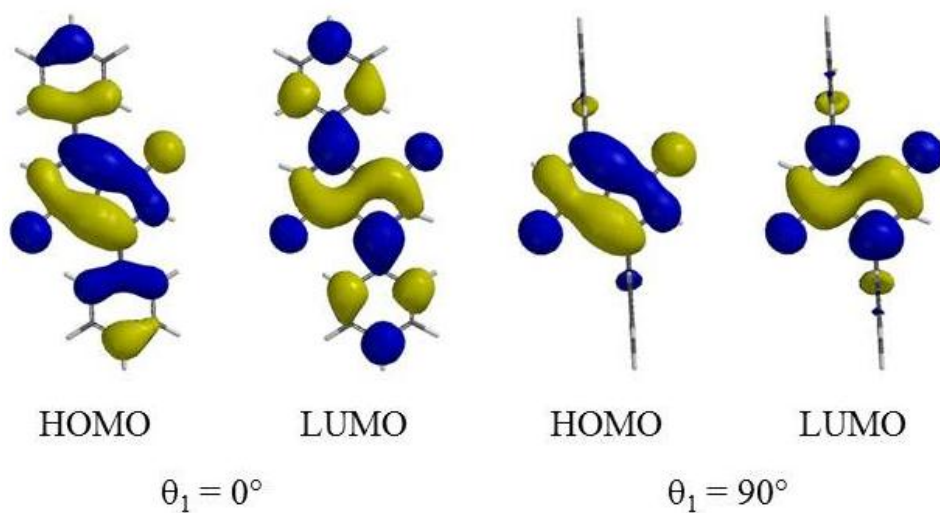


Figure 5 Highest occupied and lowest unoccupied molecular orbitals (HOMO and LUMO respectively) of neutral $\text{H}_2\text{P}_2\text{DPP}$ constrained at 0 and 90° . M06-2X/6-31G(d). IsoVal = 0.02

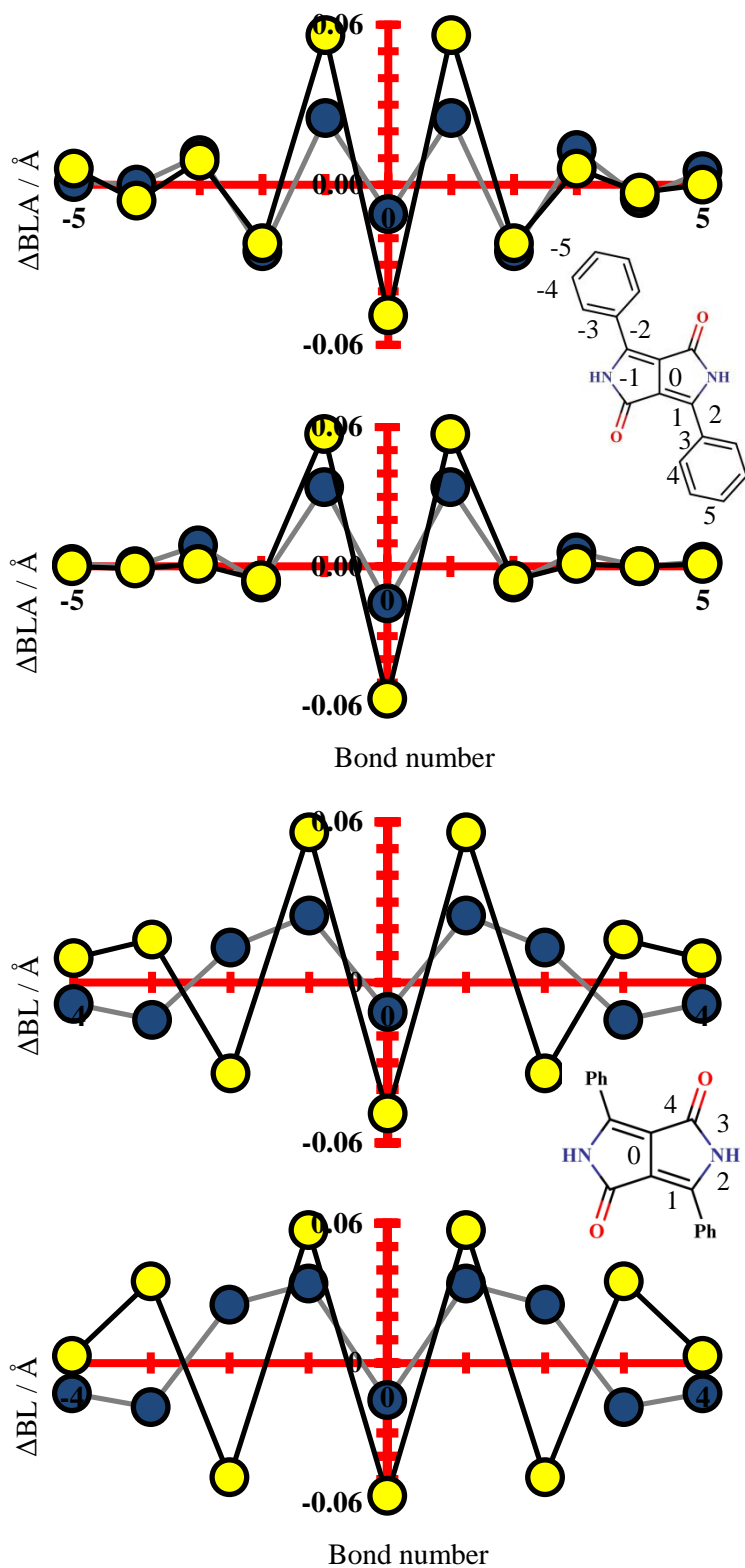


Figure 6 Plot of the difference in bond length, ΔBL between constrained Ci structures of radical cation (yellow filled circles) and radical anion (blue filled circles) and the parent neutral H_2P_2DPP versus bond number over the molecular axis as indicated by inserted structures. A and C; $\theta_1 = -\theta_2 = 0^\circ$. B and D $\theta_1 = -\theta_2 = 90^\circ$. M06-2X/6-31G(d)//M06-2X/6-31G(d).

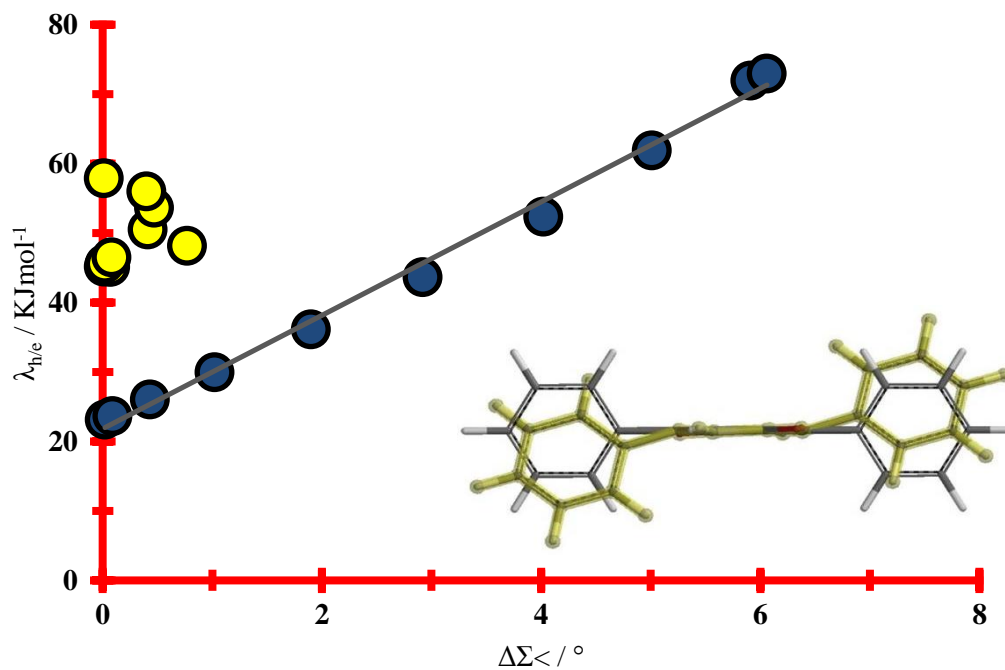


Figure 7 Plot of $\lambda_{h/e}$ as a function of the difference in the sum of C7 bond angle between radical anion (blue filled circles) and radical cation (yellow filled circles) and the neutral form for **H₂P₂DPP**. M06-2X/6-31G(d)//M06-2X/6-31G(d). Inset depicts the neutral and radical anion (highlighted) optimized geometries for $\theta_1 = -\theta_2 = 90^\circ$.

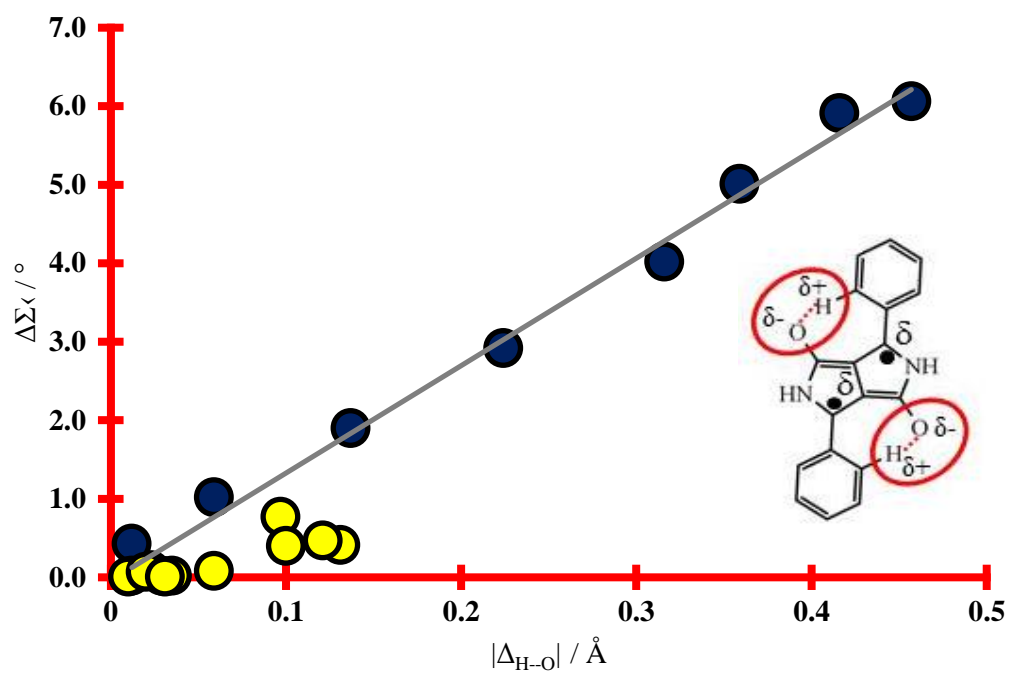


Figure 8 Plot of the difference in the sum of C7 bond angles between radical ion and neutral **H₂P₂DPP** versus O...H distance. Blue; radical anion, yellow; radical cation. Inset: structure of radical anion. The dots in anion structure are centred on the C7 atoms. M06-2X/6-31G(d)/M06-2X/6-31G(d).